The Effect of Bone Growth onto Massive Prostheses Collars in Protecting the Implant from Fracture

Paul Fromme[a], Gordon W. Blunn[b], William J. Aston[c], Tasneem Abdoola[a], Jacob Koris[b], Melanie J. Coathup[b]

[a]Department of Mechanical Engineering, University College London, Torrington Place, WC1E 7JE, London, UK

[b]Institute of Orthopaedics and Musculo-Skeletal Science, Division of Surgery & Interventional Science, University College London, Royal National Orthopaedic Hospital, Stanmore, HA7 4LP, UK.

[c]Royal National Orthopaedic Hospital, Brockley Hill, Stanmore, HA7 4LP, UK.

Corresponding author: Gordon Blunn: g.blunn@ucl.ac.uk

Keywords: Prostheses; Orthopaedics; Finite Element Analysis; HA Collar; Bone Growth

ABSTRACT

Limb-sparing distal femoral endoprotheses used in cancer patients have a high risk of aseptic loosening. It had been reported that young adolescent patients have a higher rate of loosening and fatigue fracture of intramedullary because the implant becomes undersized as patients grow. Extracortical bone growth into the grooved hydroxyapatite-coated collar had been shown to reduce failure rates. The stresses in the implant and femur have been calculated from Finite Element models for different stages of bone growth onto the collar. For a small diameter stem without any bone growth, a large stress concentration at the implant shoulder was found, leading to a significant fracture risk under normal walking loads. Bone growth onto the implant collar reduced the stress level in the implant to safe levels. For small bone bridges a risk of bone fracture was observed.

1. INTRODUCTION

Limb-sparing surgery using a massive endoprothesis has been accepted as the best choice for treatment of malignant bone tumors of the peripheral skeleton [1-3]. Longevity of the reconstruction is, however, a major concern, especially in young and active patients who place high demands on their prostheses [4]. These patients undergo neo-adjuvant chemotherapy and this has been shown to reduce recurrence of the cancer and the development of metastasis, but at the same time impairs normal bone formation. A study of custom-made distal femoral endoprotheses reported aseptic loosening as the principal mid-term mode of failure, with a 67% probability of a patient avoiding aseptic loosening for ten years [5]. In this study young patients in whom a high percentage of the femur has been replaced had the poorest prognosis for implant survival. Other studies have also shown aseptic loosening to be the major complication, with rates of loosening of distal femoral prostheses reported to be between 3% and 29% at four to ten years [5-11].

Extracortical bone bridging and osseointegration at the shoulder of the implant may reduce the risk of aseptic loosening by improving stress transfer within the cement mantle [12-16]. The formation of a pedicle of bone from the transection site onto the implant shaft has been observed in these implants and has been found to form on the medial-posterior aspect of the femur [17]. This corresponds to the site on the femur that is under compressive load. The pedicle increases in size by direct ossification. A study by Unwin et al. [18], showed the frequency and variation in the lengths of pedicle in each quadrant of the implant shoulder. Pedicle formation was shown to be more extensive on the medial and posterior quadrants with formation in the posterior quadrant being longer in length. Although bone formation in the lateral quadrant appears to result in good ossification, the frequency of occurrence is lower compared to the medial and posterior quadrants.

A number of animal and clinical studies have shown that extracortical bone-bridging can occur at the shoulder of massive bone tumor implants [19-23]. However, bone ingrowth with direct extracortical bone-implant contact in bone tumor implants retrieved from humans has only been identified in one study [24]. Extracortical bone growth into the grooved hydroxyapatite-coated collar was quantified using radiographs and histologically. Osseointegration into the collar was seen to have occurred in 66% of the patients. In these patients the success was 98% at 18 years. However, in patients where osseointegration did not occur, the failure rate was 25%.

Osseointegration may be even more important in young adolescent patients where the implant is inserted into a growing bone. Due to the small size of the bone, the implant becomes undersized as patients grow. This is due to the increase in the diameter of the endosteal cavity, which may lead to a loose implant. As loads increase as the patient grows, the stem may be too small to withstand the imposed loads and fracture may occur. An example of fracture in this region is shown in Fig.1, where fracture of the stem at the junction of the implant shaft is seen. If osseointegration into the HA collar does occur then load distribution from the implant onto the bone may bypass the stem. Using Finite Element Analysis (FEA), this study investigates the effect of bone growth onto the implant collar in the distal femur and the way in which this redistributes the stresses through the implant and bone. Quantifying the expected stresses for daily activities such as walking and comparing to the material strength improves the understanding how extensive osseointegration of the collar would protect the stem from failure. The stresses at the stem-collar junction of the implant and in the bony bridge are considered. This contribution investigates the hypothesis that with an increased bone ingrowth in the HA collar of a femoral implant, there will be a reduction in the stress (concentration) at the implant stem junction, reducing the implant fracture risk and more physiological stress transmitted between bone and implant.

2. METHODS

2.1. FE model

Finite Element models of the femoral bone and implant for different stages of bone growth onto the implant collar were developed with a rotationally symmetric geometry (Fig.2a) to approximate the observed clinical conditions for a cemented implant. The preferential pedicle growth in different quadrants (medial and posterior quadrants [18]) seen in Fig.3 was not investigated as limited information on the changing geometry was available and to limit the number of parameters. As structural failure of the implant stem is expected to occur near the transection site at the stem-collar junction, only the porous collar and stem of the implant and the distal femur were modelled. Thickness of the diaphysis was assumed to have the same outer diameter as the implant collar, i.e., 24mm. As a result of bone remodeling, particularly in young adolescent patients where growth occurs around the implant stem, less dense or porotic bone forms at the inner diameter of the cortical shell adjacent to the cement after some time [17]. This less dense layer was included with a thickness of 3 mm and models the enlarged endosteal cavity of the bone. The cement was modelled to conform to the shape of the bone on one side and the shape of the implant on the other as is realistic due to cement pressurization. Although known to vary in thickness according to the relatively rough inner bone surface, the cement was modeled as a uniform layer of 2mm thickness at the distal end. The geometry and dimensions of the implant stem and collar were modeled to mimic the Stanmore extendable prostheses and was either cylindrical with a diameter of 9mm or included a 0.75° taper in the stem (tapered stem shown in Fig.2a). This taper is a feature incorporated in many current implant designs and its effects were investigated in validating the model. A gap was kept between the bone and implant collar at the transection site as observed from radiographs (Fig.3), modelled as 1mm wide. The implant stem had a length of 150mm and the radius at the stem-collar junction was taken as 3mm.

Similarities can be drawn between the bony bridge seen at the transection site and the formation of a callus during fracture healing. The geometry of the bone formation was thus modeled as a section of a uniform semi-sphere centered at the bone-implant interface, formed of fully ossified cortical bone [25]. This led to sharp corners where the bony bridge connects to the diaphysis and implant collar. The bony bridge was modeled at 4 assumed stages of 25, 50, 75, and 100% growth (as observed from X-rays) with varying length *b* as 12,24,36,48mm and thickness *a* as 1,2,3,4mm (Fig.2a). The bridge had a respective cross-sectional area of 8, 32, 72, and 128 mm^2.

2.2. Material properties

A cylindrical axis system was defined for the model and all material properties assigned accordingly (Table 1). Transversely isotropic material properties were used for the cortical bone in the final models with the high modulus along the femoral diaphysis axis in line with its higher stiffness [25]. In order to address the effects of the bone remodeling seen in retrievals, an intermediate 'less stiff layer' between the implant-cement and cortical bone layer was modeled using trabecular bone properties as porotic bone, including a potential neocortex region adjacent to the cement. For the cement (PMMA) and implant (Ti-6Al-4V) isotropic material properties according to table 1 were assigned. For the implant, failure criteria were chosen according to [26] as 900MPa ultimate tensile strength, 830MPa yield strength, and 510MPa fatigue strength. Depending on the patient age and bone quality (density), a range of bone strength values has been reported in literature. For the cortical bone material assumed for the bony bridge experiencing high stresses a criterion of 150MPa compressive strength, towards the lower end of the range reported by [27] for human femurs, was used.

Meshes were generated in Abaqus CAE. 4-node, linear tetrahedral elements were used to represent the geometry of all parts in the model. Tetrahedral elements were chosen as they are better suited to irregular geometries such as the implant and bone formation. A localized mesh refinement sensitivity study was carried out at the radius of the collar-stem junction, where due to the cross section change stress concentration occurs. An element of edge length 1mm was chosen for the implant and bone, with a mesh refinement of element edge length 0.1mm along the radius of the implant at the stem-collar junction. A mesh of element size 0.75mm was assigned to the cement layer in order to ensure accuracy at the interfaces (Fig.2b). Small, local variations of the stress along a line of nodes was observed due to the irregular element geometry. A low-pass Butterworth filter was applied to smoothen the curves without significantly changing the shape and maximum values. For the case without bone growth the results from the FE analysis for the implant were compared to theoretical results for the stress concentration at the 3mm radius from the implant stem to the collar. The stress concentration factor was calculated based on the ratio of the 3mm radius to the stem diameter and for the chosen mesh convergence with less than 2% error was found. The FE models contained between 1.4 million elements (no bone growth) and 12 million Elements (100% growth).

2.3. Boundary conditions and loading

For the case of the implanted distal femur, the FE model was fixed at the proximal end prohibiting movement. The maximum forces recorded during a gait cycle, i.e., when the knee is fully extended, for walking was selected for use in the FE analysis and are dependent on body weight. For this study a body mass of 70kg was assumed, giving a body weight of 687N and the loads were calculated according to Taylor and Walker data [30]. Muscle forces or additional constraints were not included in the FE model, as during the surgical procedure for bone tumour prostheses in many cases the muscles around the bone are removed, even though it has been shown that their

consideration has an influence on the results [31]. A summary of the loads in the femoral axis system used [30] are shown in table 2. The investigation was carried out under a combined load as is experienced by the femur during normal activities, applied as a surface load and 4 point forces on the implant collar. This led to localized stress concentrations at the 4 point forces, but it was checked that the collar length was sufficient that this did not influence the stress results at the critical locations. It is expected that the first signs of fracture will occur at the point of maximum combined compressive stress due to the bending and axial load on the posterior-medial surface of the implant [25]. Node paths were thus defined accordingly along the Posterior-Medial surface of the implant stem. Von Mises stresses were investigated for the study in all parts of the model for consistency and can be related to the principal strain values usually evaluated for bone. Two models were initially developed where the femur was represented as transversely isotropic and isotropic. It was found that introducing anisotropy to the model had only a small effect on the stress along most of the bone (less than 2% difference), with about 7% difference at the distal end of the bone.

2.4. Implant geometry and interface conditions

The effect of a tapered implant stem compared to an un-tapered stem was investigated. As the cross-sectional area of the implant stem decreases, stress is more gradually transferred on to the bone. The tapered inner cement surface introduced a contact pressure between the cement and implant stem surfaces, preventing the implant stem from sliding longitudinally. With an un-tapered stem a relatively lower stress distribution was seen along the length of the bone (up to 10%) with an increase in stress to the same level as the un-tapered stem at the tip of the implant stem where the entire load is passed onto the bone. No change in results was seen at the stem-collar junction of the implant. A tapered stem as incorporated in many current implant designs was thus used in the FEA results reported below.

A threshold friction interaction was defined at the cement-implant interface and an independent Coulomb friction coefficient, i.e., not dependent on contact pressure between the surfaces, was assigned. A tangential friction coefficient of 0.3 was used for this investigation [32-34] and hard (penalty) contact in the normal direction. Better contact is expected at the cement-bone interface due to the cement being compressed against the relatively rough inner surface of the bone during surgery. Tissue is also known to form in the gaps between the cement and bone and hence a tied bond is assumed. All other parts are modelled as tied, i.e. cortical and porotic bone, and bone and implant collar (where appropriate). The friction model with the interface surfaces, i.e., the inner cement surface and the implant stem surface, not fully bonded, resulted in a reduced rate of stress transfer along the interface and in approximately 20% higher stresses along the surface of the implant for the friction model compared to a fully tied model.

3. RESULTS

Figure 3(b-d) shows a set of radiographs from an implanted femur over a two year period. The higher incidence of bone formation on the medial and posterior quadrants can be clearly seen. This variance in distribution of the pedicle formation could be due to a number of factors including offset loading, which may result in higher compressive stresses in the cortical bone on the posterior and medial sides or muscle insertion. Growth of the bone over the collar starts by the overgrowth of bone adjacent to the shaft over the bone. This may be associated with the formation of a radiolucent line under the shoulder of the implant. Initially a radiolucent line separates the new bone for motion but this then becomes osseointegrated. The time course for bone formation seems to be completed within 2 years after surgery. In adolescent cases where a small diameter stem was inserted due to the size of the endosteal cavity and where during growth the endosteal cavity had become larger, bone ingrowth within the HA collar seems to have

protected fixation of the implant. In the radiograph in Fig.3a (for a different patient) there is a clear radiolucency between the stem and the surrounding cortical bone, which is associated with the increase in the diameter of the endosteal cavity.

The distribution of stress in the bone and the implant is shown in Fig.4 for five geometries with 0% bone growth (Fig.4a/b), 25% bone growth (Fig.4c), 50% bone growth (Fig.4d), 75% bone growth (Fig.4e) and 100% bone growth (Fig.4f). The high stress at the implant collar end results from the load application using 4 point forces. Fig.4a for no bone growth shows the high stress concentration at the implant stem-collar transition as all stress is transmitted through the limited cross-section of the implant. Fig.4b shows the same results on a different color scale for comparison to the results for bone growth. Reduced stress in the cortical bone at the distal end of the bone interface and on the external surface of the femur compared with further along the stem (less than half) can be observed. For all stages of bone growth (Fig.4c-f) the stress at the implant stem-collar transition is reduced significantly as stress is transferred through the bony bridge onto the implant collar. With increasing bone growth the stress in the bony bridge reduced due to its increasing cross section. Stress transfer from the corner of the implant collar to the bone is visible, partially due to the assumed geometry but as well caused by the limited contact area and bone bridge thickness. Fig.5a shows a zoom of the stress distribution at the implant collar and bone growth for 25% bone growth. The highest von Mises stress in the bone at this location was recorded and is shown in Fig.5b for the assumed 4 stages of bone growth. The recorded stress reduced from 235 MPa for 25% bone growth to 65MPa for 100% bone growth.

Von Mises stresses were analyzed along the posterior medial surface of the implant and the maximum stresses were found to occur at 27mm along the length of the implant at the stem-collar junction (Fig.6). The stress at this point on the surface was recorded for the five geometries of

bone growth. Maximum values for the FE models are shown in table 3 and the relevant parameters to detect risk of fracture for medical titanium alloy (Ti-6Al-4Va) were stated in the material properties section. The distribution of stress along the stem of the implant is shown graphically in Fig.6.

4. DISCUSSION

The ultimate tensile strength represents the stress value at which the implant will fracture, e.g. during a sideways fall or stumbling, which can lead to very high, but difficult to predict loads. As the knee joint is exposed to cyclic loading due to daily activities such as walking, the yield and fatigue strength are relevant in predicting fatigue failure of the implant. Bone growth onto the implant collar was modeled with rotational symmetry, as limited geometrical information on preferential pedicle growth was available and to limit the number of parameters. Preferential bone pedicle growth in different quadrants around the circumference was not investigated. The results shown in Fig.6 indicate that the stresses on the surface of the implant stem are highest when there is no growth into the collar. In comparing the values of table 3 with the stress limits for ultimate tensile strength, yield strength and fatigue strength respectively, it is clear that an implant sized for a young patient with no bone growth under the full adult bodyweight load of 687N would almost definitely fail due to structural failure at the implant stem-collar junction during the normal daily activity of walking as the maximum stress exceeds the material strength. It is also observed from table 3 and Fig.6 that bone growth and attachment to the implant collar results in a reduction in the peak stresses (factor approximately 4) and protects the implant from structural failure. The least amount of bone growth, i.e. 25%, causes a reduction in stress of the order of approximately 800MPa immediately removing the risk of fracture, yield or fatigue. This conclusion holds for both tie and friction models, as well as isotropic or anisotropic material properties. Loads transmitted through the implanted bone were reduced when compared to that of an un-implanted

bone. This finding is consistent with the clinical results of bone resorption around implanted stems in clinical practice. The preferential load-carrying of the stiff implant is responsible for the lowered stresses recorded in the femur. This result is compounded when the bone and metal are intimately attached and as we modeled the attachment as a perfect bond, it is likely that the recorded difference in stress between bone and implant was larger than in physiological conditions where the contact will be imperfect [35].

For a small bony bridge onto the HA collar (25% growth, thickness 1mm) a maximum stress of 235MPa in the bone was recorded at the corner with the implant collar. While the stress concentration might be overestimated due to the chosen FE model geometry, this value is significantly higher than the compressive strength of femoral bone reported in literature (approximately 150MPa [27]) and a risk of fracture of the small bone growth onto the HA collar exists. For all considered larger cases of bone growth the maximum stress at this location of the bone was reduced significantly below the compressive bone strength. This shows the importance of good bone growth onto the implant collar to protect both the bone and implant from the risk of fracture due to walking loads for the larger weight of an adult patient.

A study by Agarwal et al [36] of femoral megaprostheses in developing countries recorded 28 occurrences of implant fracture. 21 of these fractures occurred at the stem-collar junction. Finite element analysis showed that this was the region of highest stress. This clinical finding was consistent with the results recorded from the surface of the implant, as stress peaks were always present at the stem-collar junction, making this point the most likely to fail under high loads. Recent radiographic and histological study investigating bone ingrowth into a HA collar in the distal femoral implants used to treat patients of all ages showed increased survivorship and reduced radiolucent line progression when osseointegration at the shoulder could be identified

compared to implants where ingrowth was not evident [24, 37].

Non-invasive extendable prostheses can provide excellent post-operative functionality and cosmetic appearance for patients who have had large joint resection without jeopardizing the oncological safety margin. As with all surgery, complications can lower the life expectancy of the implant. Stem fracture, bone fracture and loosening are very serious complications, which necessitate revision of the implant, or surgical intervention. Loosening in young adolescent patients is associated with growth. As a patient grows the endosteal cavity increases in diameter, leaving weak bone to support the implant that fails leading to loosening [17]**.** Additionally the stem that is inserted into a young patient has a small diameter due to the geometry of the femur, but as the patient grows and loads passing through the implant increase, then the stem is at risk of fracture.

In this study we have shown that bone growth over the collar of an implant reduces the magnitude of stress in the stem of the implant. This effect is most noticeable at the stem-collar junction where stress concentration occurs. This is the site of most mechanical failures due to fatigue fracture. Therefore, it is possible that bone growth over the collar will protect the stem from large stress concentrations, reducing the risk of stem fracture or implant loosening.

Bone resorption due to stress shielding is another common complication of massive endoprotheses. This can lower the strength of the bone, lead to implant loosening, and increase the risk of fracture. This occurs when there is a reduction in stress through the bone and in our model was seen in cases where there was no bone ingrowth into the collar. We have shown that osseointegration of the collar increases the stress in the proximal bone when compared to implanted bone without a collar. Small amounts of osseointegration show high levels of bone

stress, which decrease as osseointegration increases. Stress along the implant was always increased when the bone was unattached to the collar of the implant compared to conditions that modeled bone integration at this point. Looking at studies of stem fracture of total hip replacements, it may be the case that the increased stress, experienced when a gap is created between the bone and the stem, may increase the likelihood of the stress reaching the endurance limit leading to fatigue fracture. We have shown that ingrowth into the HA Collar alleviates stress concentrations in this region and this is a particularly important finding when using these implants in young patients. Therefore, surgeons and designers must strive to enhance ingrowth into this region of the implant. The efficacy of different methods to promote osseointegration of the collar (e.g. surface design, implant and material stiffness, coatings) should be further investigated to provide guidance.

ACKNOWLEDGEMENTS

G.W. Blunn is co-founder of a company (Stanmore Implants Worldwide) that manufactures bone tumor implants. W. Aston is an orthopaedic surgeon specializing in the treatment of bone cancer who uses massive bone implants. Part-funding was received from Orthopaedic Research UK.

REFERENCES

1. Jeys LM, Kulkarni A, Grimer RJ, et al. Endoprosthetic reconstruction for the treatment of musculoskeletal tumors of the appendicular skeleton and pelvis. J Bone Joint Surg Am 2008;90:1265-71.
2. Myers GJC, Abudu AT, Carter SR, et al. The long-term results of endoprosthetic replacement of the proximal tibia for bone tumours. J Bone Joint Surg Br 2007;89:1632-7.

3. Kawai A, Lin PP, Boland PJ, et al. Relationship between magnitude of resection, complication, and prosthetic survival after prosthetic knee reconstructions for distal femoral tumors. J Surg Oncol 1999;70:109-15.
4. Farfalli GL, Boland PJ, Morris CD, et al. Early equivalence of uncemented press-fit and compress femoral fixation. Clin Orthop Relat Res 2009;467:2792-9.
5. Unwin PS, Cannon SR, Grimer RJ, et al. Aseptic loosening in cemented custom-made prosthetic replacements for bone tumours of the lower limb. J Bone Joint Surg Br 1996;78:5-13.
6. Mittermayer F, Krepler P, Dominkus M, et al. Long-term followup of uncemented tumor endoprostheses for the lower extremity. Clin Orthop Relat Res 2001;388:167-77.
7. Torbert JT, Fox EJ, Hosalkar HS, et al. Endoprosthetic reconstructions: results of long-term followup of 139 patients. Clin Orthop Relat Res 2005;438:51-9.
8. Gosheger G, Gebert C, Ahrens H, et al. Endoprosthetic reconstruction in 250 patients with sarcoma. Clin Orthop Relat Res 2006;450:164-71.
9. Griffin AM, Parsons JA, Davis AM, et al. Uncemented tumor endoprostheses at the knee: root causes of failure. Clin Orthop Relat Res 2005;438:71-9.
10. Guo W, Ji T, Yang R, et al. Endoprosthetic replacement for primary tumours around the knee: experience from Peking University. J Bone Joint Surg Br 2008;90:1084-9.
11. Ahlmann ER, Menendez LR, Kermani C, Gotha H. Survivorship and clinical outcome of modular endoprosthetic reconstruction for neoplastic disease of the lower limb. J Bone Joint Surg Br 2006;88:790-5.
12. Saran N, Zhang R, Turcotte RE. Osteogenic protein-1 delivered by hydroxyapatite-coated implants improves bone ingrowth in extracortical bone bridging. Clin Orthop Relat Res 2011;469:1470-8.

13. Chao EY, Sim FH. Composite fixation of segmental bone/joint defect replacement (SDR) prostheses. Biological and biomechanical justifications. Chir Organi Mov 1990;75(Suppl):171-3.
14. Chao EY, Fuchs B, Rowland CM, et al. Long-term results of segmental prosthesis fixation by extracortical bone-bridging and ingrowth. J Bone Joint Surg Am 2004;86:948-55.
15. Chao EY, Sim FH. Composite fixation of salvage prostheses for the hip and knee. Clin Orthop Relat Res 1992;276:91-101.
16. Tanzer M, Turcotte R, Harvey E, Bobyn JD. Extracortical bone bridging in tumor endoprostheses. Radiographic and histologic analysis. J Bone Joint Surg Am 2003;85:2365-70.
17. Blunn GW, Wait ME. Remodelling of bone around intramedullary stems in growing patients. J Orthop Res 1991;9:809-19.
18. Unwin PS, Cobb JP, Walker PS. Distal femoral arthroplasty using custom-made prostheses: The first 218 cases. J Arthroplasty 1993;8:259-68.
19. Heck DA, Chao EY, Sim FH, et al. Titanium fibermetal segmental replacement prostheses. A radiographic analysis and review of current status. Clin Orthop Relat Res 1986;204:266-85.
20. Kuo KN, Gitelis S, Sim FH, et al. Segmental replacement of long bones using titanium fiber metal composite following tumor resection. Clin Orthop Relat Res 1983;176:108-14.
21. Heck DA, Nakajima I, Kelly PJ, Chao EY. The effect of load alteration on the biological and biomechanical performance of a titanium fiber-metal segmental prosthesis. J Bone Joint Surg Am 1986;68:118-26.
22. Ward WG, Johnston KS, Dorey FJ, Eckardt JJ. Extramedullary porous coating to prevent diaphyseal osteolysis and radiolucent lines around proximal tibial replacements. A preliminary report. J Bone Joint Surg Am 1993;757:976-87.

23. Okada Y, Suka T, Sim FH, et al. Comparison of replacement prostheses for segmental defects of bone. Different porous coatings for extracortical fixation. J Bone Joint Surg Am 1988;702:160-72.
24. Coathup MJ, Batta V, Pollock RC, et al. Long-term survival of cemented distal femoral endoprostheses with a hydroxyapatite-coated collar: a histological study and a radiographic follow-up. J Bone Joint Surg Am 2013;95:1569-75.
25. Carter DR, Beaupré GS, Giori NJ, Helms JA. Mechanobiology of skeletal regeneration. Clin Orthop Relat Res 1998;355(Suppl):S41-S55.
26. Kutz M, editor. Mechanical Engineers' Handbook: Materials and Mechanical Design. Hoboken: Wiley, 2006, p 221-54.
27. Yamada H. Aging rate for the strength of human organs and tissues. In: Evans FG, editor. Strength of Biological Materials. Baltimore: Williams and Wilkins; 1970, p 272-280.
28. Newcombe L, Dewar M, Blunn GW, Fromme P. Effect of amputation level on the stress transferred to the femur by an artificial limb directly attached to the bone. Med Eng Phys 2013;35:1744-53.
29. Krone R, Schuster P. An investigation on the importance of material anisotropy in Finite-Element modeling of the human femur. SAE Technical Paper 2006;01-0064.
30. Taylor SJG, Walker PS. Forces and moments telemetered from two distal femoral replacements during various activities. J Biomech 2001;34:839-48.
31. Bayoglu R, Okyar AF. Implementation of boundary conditions in modeling the femur is critical for the evaluation of distal intramedullary nailing. Med Eng Phys 2015; 37:1053-60.
32. Mann KA, Bartel DD, Wright TM, Ingraffea AR. Mechanical characteristics of the stem-cement interface. J Orthop Res 1991;9:798-808.

33. Nuño N, Amabili M, Groppetti R, Rossi A. Static coefficient of friction between Ti-6Al-4V and PMMA for cemented hip and knee implants. J Biomed Mater Res 2002;59:191-200.
34. Completo A, Fonseca F, Simoes JA. Experimental validation of intact and implanted distal femur Finite Element models, J Biomech 2007;40:2467-76.
35. Engh CA, Bobyn JD, Glassman AH. Porous-coated hip replacement. The factors governing bone ingrowth, stress shielding, and clinical results. J Bone Joint Surg Br 1987;69:45-55.
36. Agarwal M, Gulia A, Ravi B, Ghyar R. Revision of broken knee megaprostheses new solution to old problems. Clin Orthop Relat Res 2010;468:2904-13.
37. Coathup MJ, Sanghrajka A, Aston WJ, et al. Hydroxyapatite-coated collars reduce radiolucent line progression in cemented distal femoral bone tumor implants. Clin Orthop Relat Res 2015;473:1505-14.

FIGURE LEGENDS

Figure 1. X-ray of fractured stem showing fracture at the shoulder of an implant with no evidence of bone ingrowth for tibia in lower leg.

Figure 2. (a) Schematic of Finite Element model geometry (all dimensions in mm); bone formation onto implant collar with dimensions (a and b); (b) FE mesh for 75% growth.

Figure 3. (a) M-L radiograph of patient taken 12 years after prostheses implanted at age of 7 years; M-L views [left] and A-P views [right] of set of x-rays from implanted femur for different patient taken: (b) immediately post surgery; (c) one year post surgery; (d) two years post surgery.

Figure 4. Contour plot of stress distribution (von Mises) in FE model (bone and implant): (a) no growth [scale 0-500MPa]; (b) no growth; (c) 25% growth; (d) 50% growth; (e) 75% growth; (f) 100% growth [all scale 0-100MPa].

Figure 5. (a) Zoom of contour plot of stress distribution at implant collar and bone growth: (b) maximum stress (von Mises) in bone close to implant collar for different stages of bone growth.

Figure 6. Von Mises stress along medial-posterior surface of implant for stages of bone growth onto the implant collar): no growth (red, solid); 25% growth (black, solid); 50% growth (purple, dash-dotted); 75% growth (green, dashed); 100% growth (blue, solid).

Figure 1

Figure 2

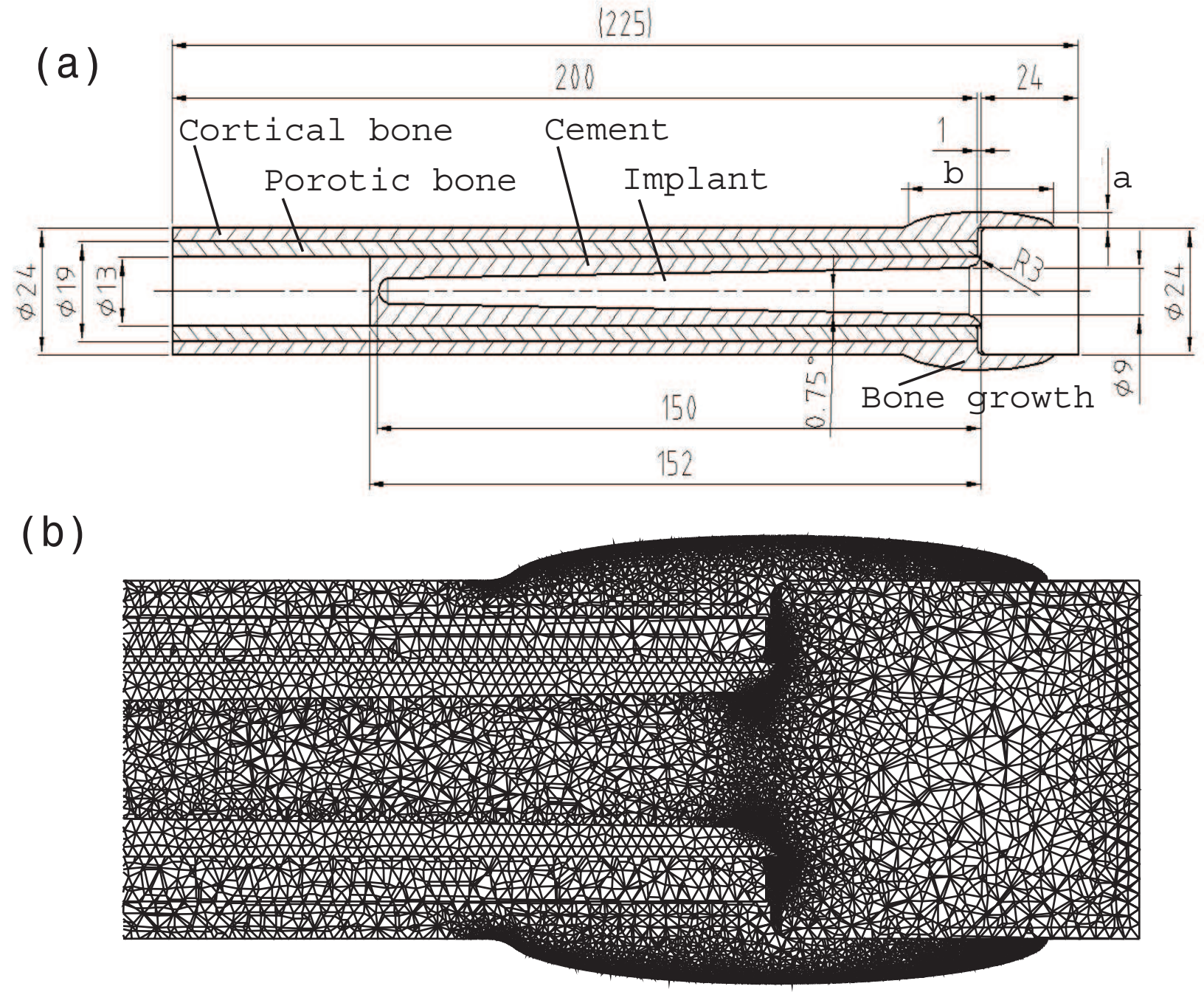
(a)
(225)
200
24
Cortical bone
Porotic bone
Cement
Implant
1
b
a
R3
ϕ24
ϕ19
ϕ13
ϕ24
ϕ9
0.75°
Bone growth
150
152
(b)

Figure 3

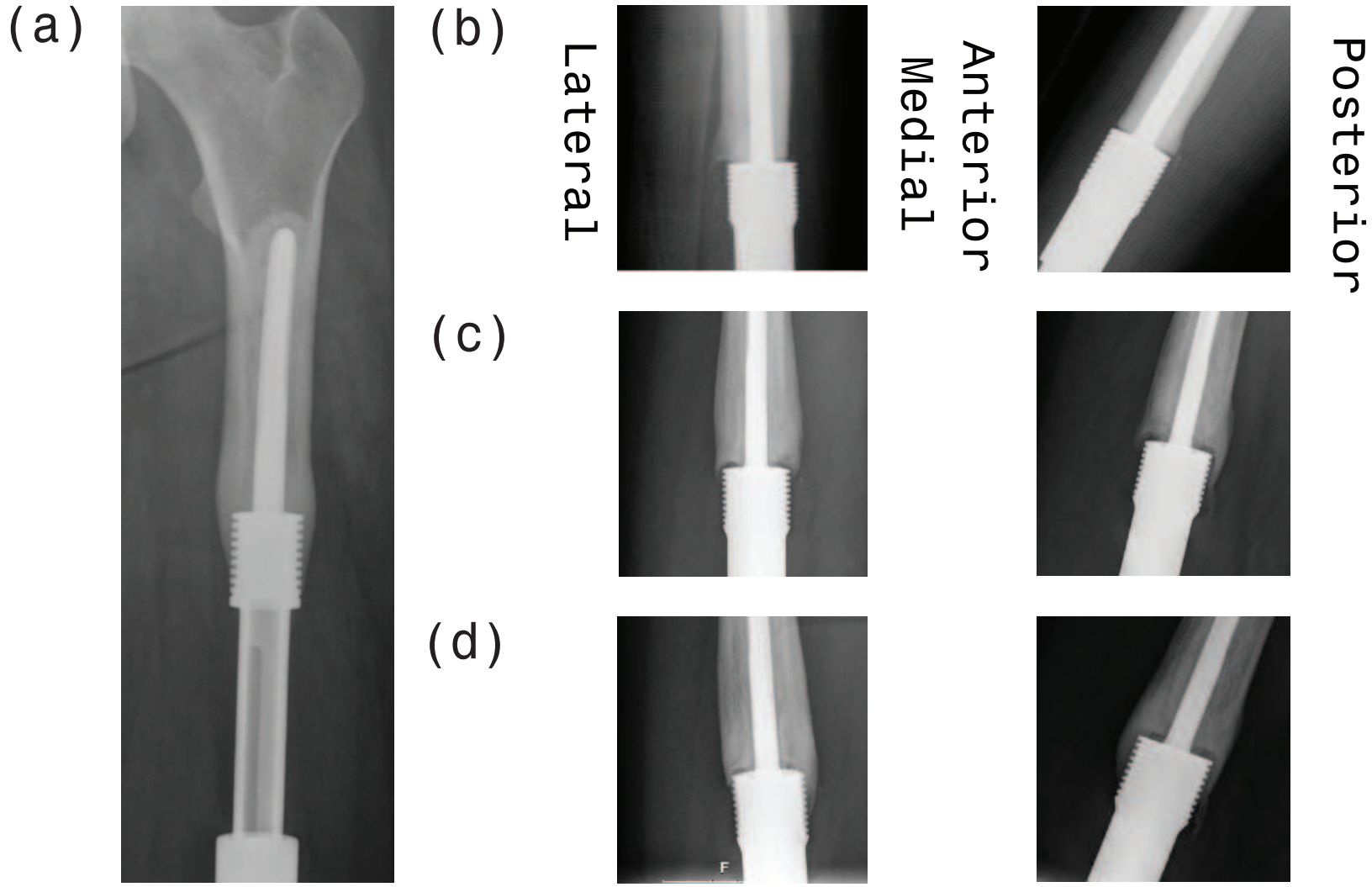

Figure 4

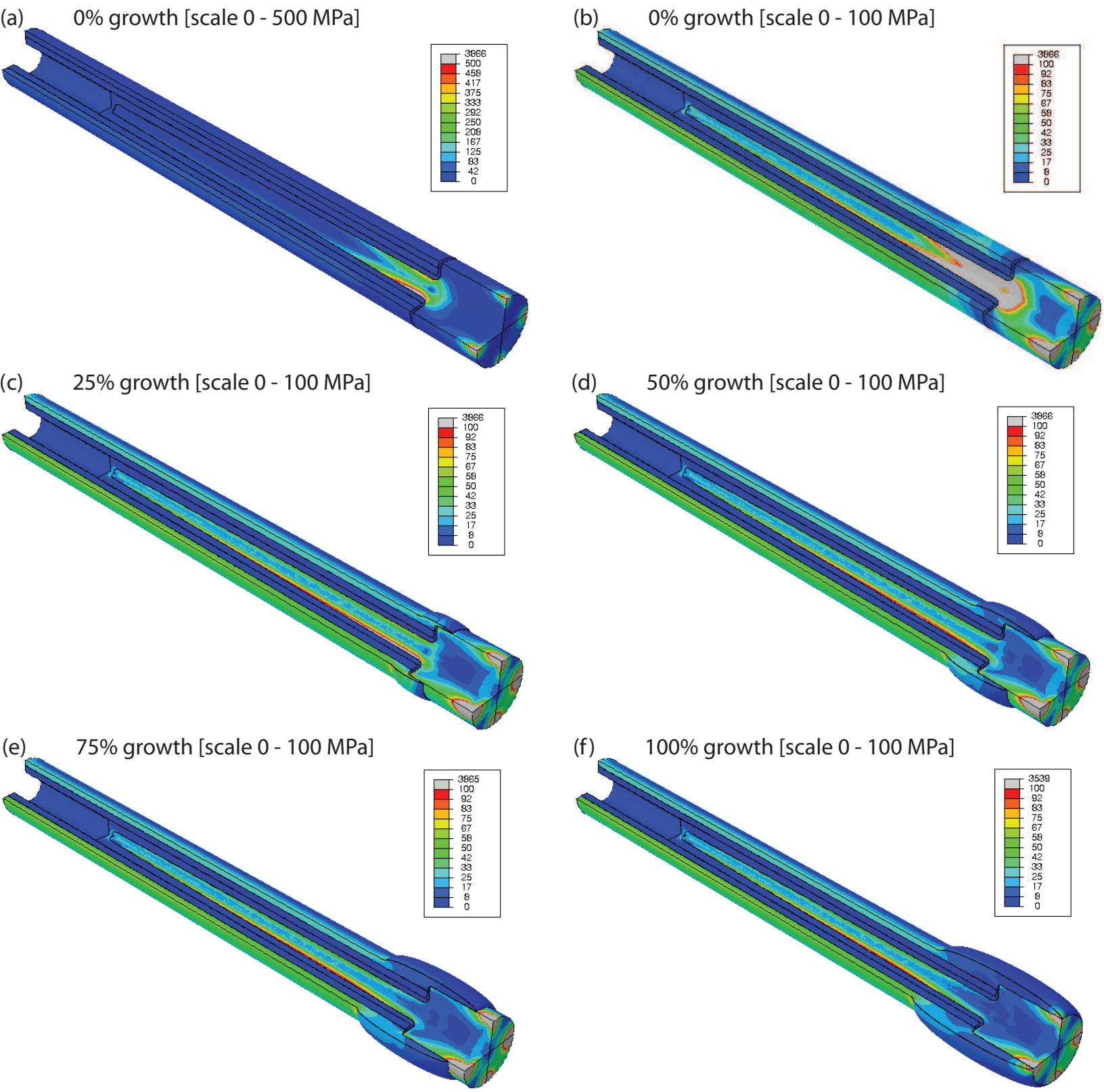
(a) 0% growth [scale 0 - 500 MPa]
3866
500
458
417
375
333
292
250
208
167
125
83
42
0
(b) 0% growth [scale 0 - 100 MPa]
3866
100
92
83
75
67
58
50
42
33
25
17
8
0
(c) 25% growth [scale 0 - 100 MPa]
3866
100
92
83
75
67
58
50
42
33
25
17
8
0
(d) 50% growth [scale 0 - 100 MPa]
3866
100
92
83
75
67
58
50
42
33
25
17
8
0
(e) 75% growth [scale 0 - 100 MPa]
3865
100
92
83
75
67
58
50
42
33
25
17
8
0
(f) 100% growth [scale 0 - 100 MPa]
3539
100
92
83
75
67
58
50
42
33
25
17
8
0

Figure 5

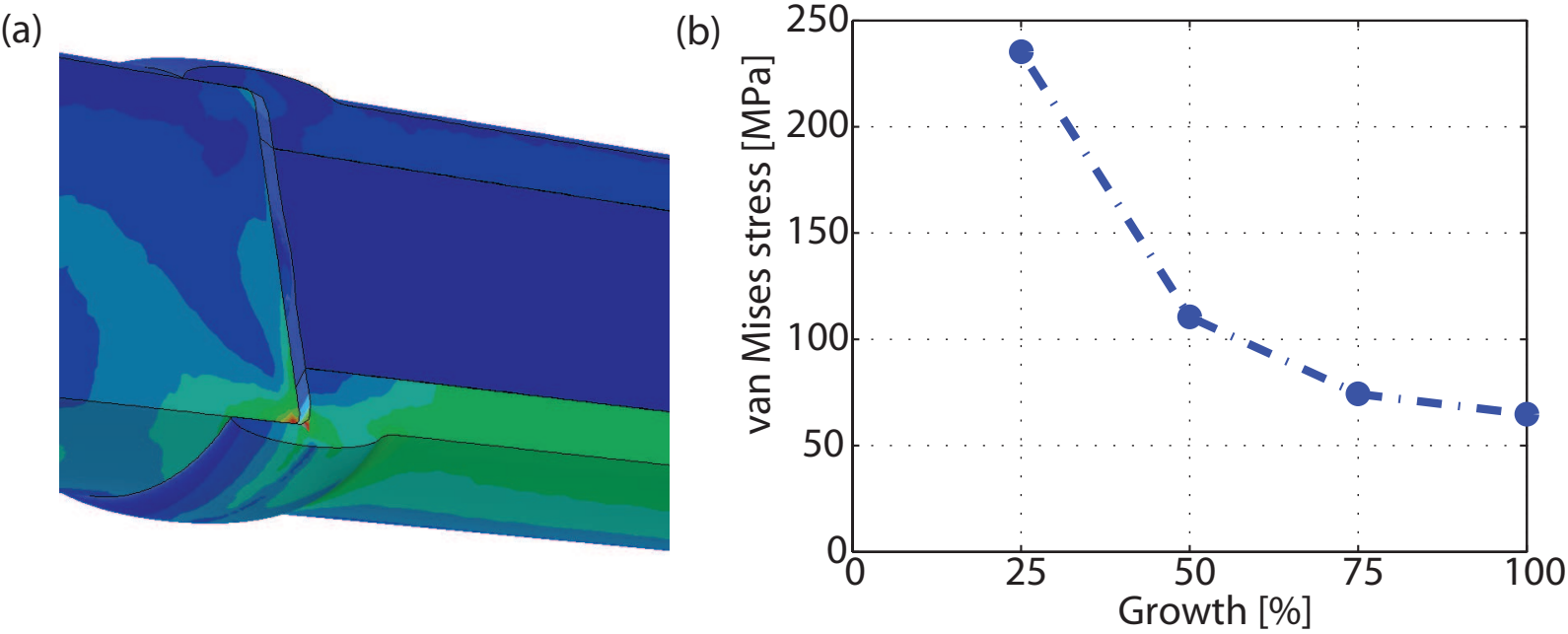
(a)
(b)
250
200
150
100
50
0
van Mises stress [MPa]
0
25
50
75
100
Growth [%]

Figure 6

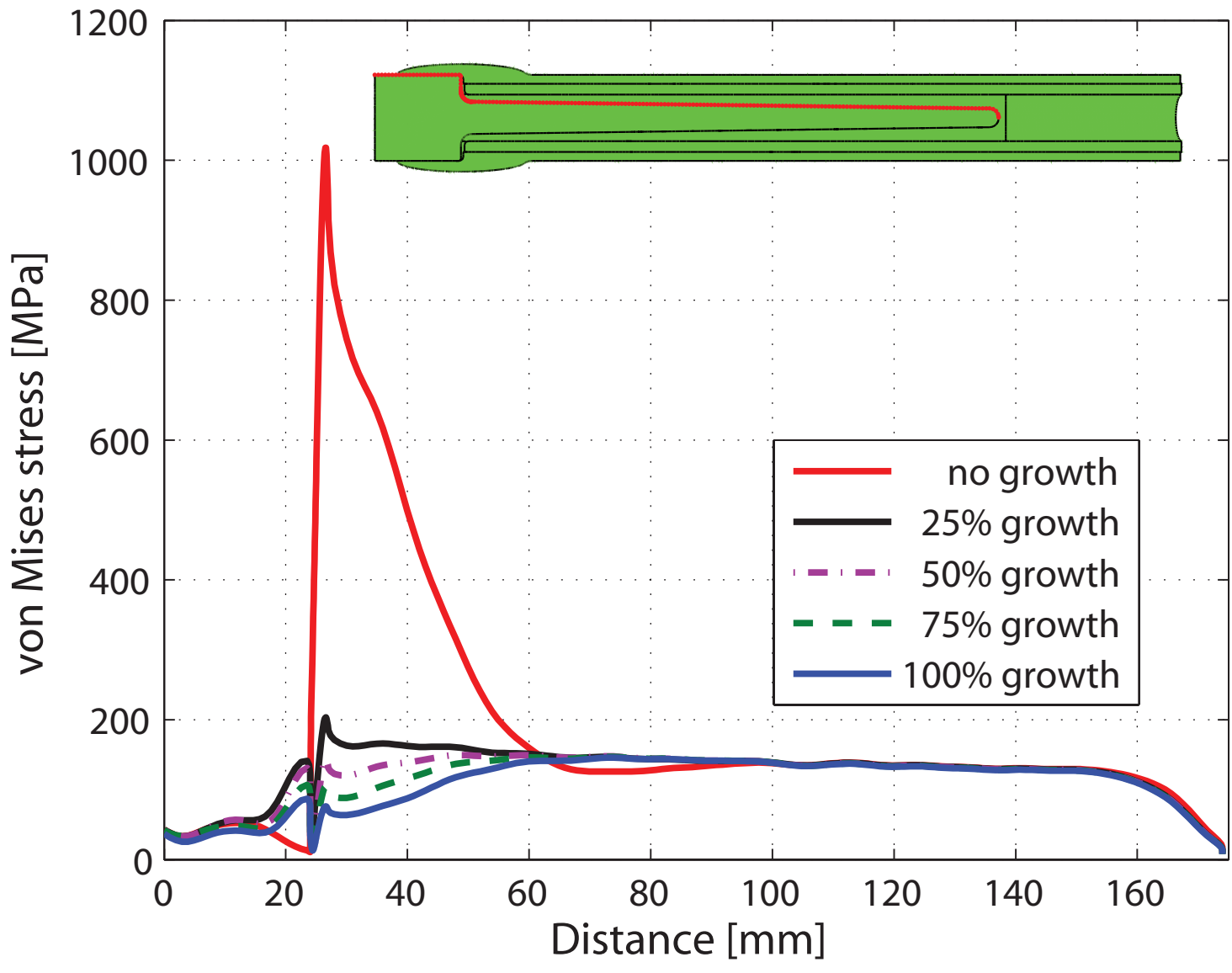
1200
1000
800
600
400
200
0
0
20
40
60
80
100
120
140
160
von Mises stress [MPa]
Distance [mm]
no growth
25% growth
50% growth
75% growth
100% growth

Table 1: Material properties for implant and PMMA cement used in FE model (according to [26]), cortical bone transversely isotropic material properties (adapted from [28]), porotic bone transversely isotropic material properties (according to [29]).

Part		**Young's Modulus (GPa)**	**Poisson's ratio (v)**	**Shear Modulus (GPa)**
Implant (Ti-6Al-4V)		E=110	v=0.3	N/A
PMMA Cement		E=3.10	v=0.4	N/A
Cortical Bone	**Longitudinal**	E3=20.0	v12=0.376	G12=4.53
	Transverse	E1=12.0	ν23=0.235	G23=6.23
		E2=12.0	V13=0.376	G13=4.53
Porotic Bone	**Longitudinal**	E3=1.352	v12=0.3	G12=0.399
	Transverse	E1=0.822	ν23=0.3	G23=0.370
		E2=0.822	V13=0.3	G13=0.399

Table 2: Walking loads applied to FE model (calculated from [30]).

Recorded Load	Axial Load	AP Bend	ML Bend	Torsion
Body weight	3.3 BW	96 BWmm	57 BWmm	6 BWmm
Applied Load	2267 N	66 Nm	39 Nm	4.1 Nm

Table 3: Von Mises stress (MPa) at stem-collar junction of the implant.

% Bone Growth	Stress [MPa]
0	1018
25	203
50	143
75	104
100	76